Cancer Management and Research

Elevate Series

Open Access Full Text Article

ORIGINAL RESEARCH

Development and Validation of a Radiomics Nomogram Based on Magnetic Resonance Imaging and Clinicoradiological Factors to Predict HCC TACE Refractoriness

YuHan Dong[1], Jihong Hu[2], Xuerou Meng[2], Bin Yang[3], Chao Peng[1], Wei Zhao[1]

[1]Medical Imaging Department, The First Affiliated Hospital of Kunming Medical University, Kunming, 650032, People's Republic of China; [2]Department of Interventional Radiology, The First Affiliated Hospital of Kunming Medical University, Kunming, 650032, People's Republic of China; [3]Medical Imaging Center, The First Hospital of Kunming, Kunming, 650051, People's Republic of China

Correspondence: Wei Zhao; Chao Peng, Medical Imaging Department, The First Affiliated Hospital of Kunming Medical University, Kunming, 650032, People's Republic of China, Email kyyyzhaowei@foxmail.com; 609101429@qq.com

Purpose: This study constructs a predictive model for hepatocellular carcinoma (HCC) transarterial chemoembolization (TACE) refractoriness using a machine learning (ML) algorithm and verifies the predictive performance of different algorithms.

Patients and Methods: Clinical and magnetic resonance imaging (MRI) data of 131 patients (48 with TACE refractoriness) who underwent repeated TACE treatment for HCC were retrospectively collected. The training and validation cohorts comprised 104 and 27 cases, respectively, following an 8:2 ratio. Clinical imaging characteristics related to TACE refractoriness were identified through logistic regression analysis. HCC lesions on arterial phase, portal phase, delayed phase, and T2-weighted fat suppression MRI images before the first TACE were manually delineated as regions of interest. Dimension reduction was conducted using variance threshold, univariate selection, and least absolute shrinkage and selection operator methods. Relevant indices of TACE refractoriness were selected. ML algorithms, including a support vector machine, random forest, logistic regression and adaptive boosting, were used to construct the radiomics, clinical prediction, and combined models. The predictive performance of these models was evaluated using receiver operating characteristic curves. The optimal model was presented as a nomogram and verified through calibration and decision curve analyses.

Results: In evaluating radiomics models for predicting TACE refractoriness in HCC, the LR-developed portal venous phase (VP) model achieved optimal single-sequence performance (training AUC: 0.896, 95% CI: 0.843–0.941; validation: 0.853, 0.727–0.965). Multisequence models significantly surpassed single-sequence counterparts, with the T2WI-FS+AP+VP+DP multisequence LR model demonstrating peak efficacy (training: 0.905, 0.853–0.949; validation: 0.876, 0.773–0.976). The integrated clinical-radiomics model demonstrated robust predictive performance, achieving a training cohort AUC of 0.955 (95% CI: 0.918–0.984) with 0.885 accuracy, 0.921 sensitivity, and 0.864 specificity, and maintained strong validation performance (AUC=0.941, 95% CI: 0.880–0.991).

Conclusion: Multisequence clinical-radiomics model accurately predicts TACE refractoriness in hepatocellular carcinoma.

Keywords: hepatocellular carcinoma, machine learning, transarterial chemoembolization, radiomics

Introduction

Transarterial chemoembolization (TACE) is a common treatment for malignant hepatic tumors, particularly advanced liver cancer. It plays a role in down-staging, bridging, providing palliative care, and treating earlier stages of hepatocellular carcinoma (HCC), Complete embolization with a single blood supply and super-selective intubation can potentially achieve radical treatment.[1,2] However, due to the heterogeneity of HCC and the limitations of TACE, some patients do not benefit from TACE treatment, and repeated ineffective TACE treatment can lead to reduced efficacy, tumor progression, and liver function damage.[2] In 2010, the Japan Society of Hepatology (JSH) first proposed the concept of "TACE refractoriness" to identify this condition early and adjust treatment strategies accordingly. This concept was further refined in 2014 and remains in use today.[3] Various countries have also defined TACE refractoriness, such as the

Received: 11 July 2024
Accepted: 29 June 2025
Published: 17 July 2025

Expert Panel Opinion on Interventions in Hepatocellular Carcinoma,[4] the European Association for the Study of the Liver,[5] and the Annual Meeting of Chinese College of Interventionalists.[6] Previous studies on TACE refractoriness have struggled to form a unified and consistent evaluation,[6] and the assessment of refractoriness was made only after two to three ineffective TACE treatments, inevitably delaying the transition to and optimization of effective therapies. Rigorous scientific research and demonstrations are needed to detect and predict TACE refractoriness promptly, ensuring the best possible treatment opportunities.

Currently, various expert consensus clinical judgments are evaluated based on imaging manifestations. With the rapid development of artificial intelligence in medical imaging, the evaluation of HCC TACE refractoriness has evolved from efficacy evaluations based on clinical data to radiomics studies incorporating extensive tumor information from imaging, significantly improving prediction efficiency. Radiomics provides quantitative analysis of tumor heterogeneity and early treatment response prediction, overcoming the subjective limitations of conventional imaging.[7] This study aimed to construct a combined model using MRI radiomics to analyze MRI images of patients with HCC before their initial TACE, predict and identify patients with HCC showing TACE refractoriness, and guide timely adjustments to treatment plans.

Materials and Methods

Patients

Clinical and imaging data of patients with HCC treated with TACE were collected from the Interventional Department of the First Affiliated Hospital of Kunming Medical University from January 1, 2017, to December 31, 2019.

This retrospective study was approved by the Ethics Committee of the First Affiliated Hospital of Kunming Medical University (Approval No. 2024-L-105) and adhered to the ethical principles of the Declaration of Helsinki. Given the non-interventional retrospective design, the requirement for informed consent was formally waived. All patient data were anonymized prior to analysis through the removal of personal identifiers to ensure confidentiality. Inclusion criteria were as follows: patients who (1) met the Guidelines for Diagnosis and Treatment of Primary Liver Cancer (2022 Edition),[1] (2) were aged between 18 and 80 years at the first diagnosis, (3) underwent an MRI plain scan and enhancement 1 week before the first TACE, (4) received TACE twice consecutively or achieved complete response (CR) after TACE treatment despite receiving only one TACE treatment, and (5) received no treatment for HCC before TACE (ie, surgical resection, RFA, HAIC, and immuno-targeted therapy). Exclusion criteria were as follows: (1) an interval between the first and second TACE exceeding three months, (2) the presence of diffuse liver cancer or other cancers, (3) incomplete data (irregular follow-up/lack of clinical imaging data), and (4) unmeasurable lesions (Figure 1).

Follow-Up and Grouping

The assessment included tumor markers, liver function tests, abdominal computed tomography/magnetic resonance imaging (MRI) scans, and other necessary laboratory tests. The postoperative efficacy of TACE was evaluated using mRECIST criteria. mRECIST evaluates the effectiveness of the entire HCC disease rather than solely the target lesion, and in order to increase the imaging phenotype and sample variables in the radiomics evaluation studies. The target lesion comprised the middle segments I and IV of the liver as the center. This study adopted the JSH definition of TACE refractoriness,[3] defined as follows: (1) Despite changing chemotherapy drugs or reevaluating tumor blood supply, MRI examination performed 1 to 3 months after two or more consecutive TACE treatments shows more than 50% of active lesions remaining in the liver or new lesions appearing; (2) extrahepatic metastasis or vascular invasion; (3) tumor markers continuing to rise after TACE. Patients with HCC who met the criteria or were followed up after CR for initial postoperative efficacy assessment were categorized into a TACE refractoriness group and a TACE effective group.

Treatment Methods

A 5F YASHIRO catheter (7750070148/5F, 70 cm, Hunan APT Medical Equipment Co., Ltd.) was inserted into the celiac artery through the femoral artery using the Seldinger technique to identify the blood supply. If necessary, angiography of the superior mesenteric or phrenic artery was conducted. Lipiodol emulsion and chemotherapeutic drugs (oxaliplatin,

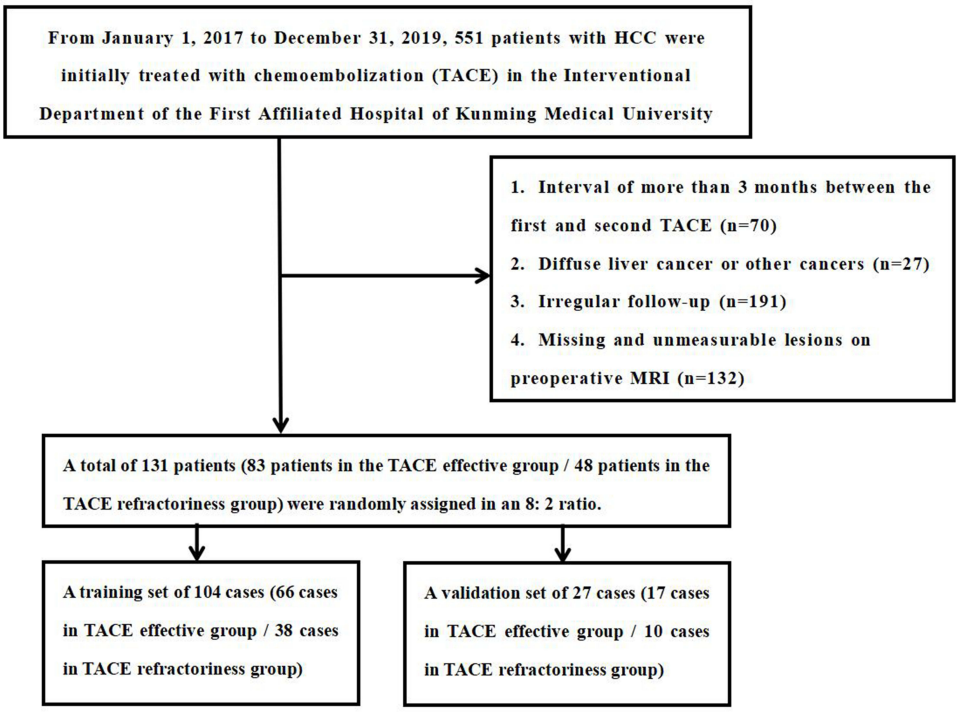

Figure 1 Flow chart of inclusion and exclusion criteria.

Sanofi Co., Ltd.; epirubicin, Zhejiang Hisun Pharmaceutical Co., Ltd.) or 50 mg of epirubicin (Zhejiang Hisun Pharmaceutical Co., Ltd.) were loaded into 100–300 μm drug-eluting beads (CalliSpheres, Jiangsu Hengrui Medicine Co., Ltd.) to form a microsphere suspension. The microsphere suspension was injected into the feeding artery of the tumor using a 2.6 F microcatheter (MS-C26G21AS5 Jiangsu Hengrui Medicine Co., Ltd.) until the blood flow was significantly reduced. Finally, embolization was performed using polyvinyl alcohol microspheres and gelatin sponge particles as required. During this process, attention should be paid to the redistribution of microspheres. Angiography was repeated for at least 5 min after embolization to assess its effectiveness. Satisfactory embolization is indicated by the disappearance of tumor staining and cessation of blood. Given the varied disease stages in the study, treatment targets were determined according to specific conditions, avoiding unnecessary embolization of surrounding normal liver tissue, and treatment targets were achieved.[8]

Image Data Acquisition

All included patients underwent plain and enhanced MRI scans before the initial TACE (Table 1). The collection sequences included T2-weighted imaging fat suppression (T2WI-FS), arterial phase (AP), portal vein phase (VP), and

Table 1 MRI Equipment Parameters

Equipment	Imaging Sequence	TR (ms)	TE (ms)	FOV (mm^2)	Matrix Size
1.5T GE (80 cases)	T2WI-FS	6000	81	400 × 400	320 × 190
	T1WI-DCE	3.5	1.7	400 × 400	320 × 224
3.0T GE (12 cases)	T2WI-FS	8571	93	380 × 380	320 × 320
	T1WI-DCE	4.3	1.7	380 × 380	288 × 208
1.5T SIEMENS (25 cases)	T2WI-FS	5253	90	400 × 300	320 × 240
	T1WI-DCE	4.21	1.9	400 × 300	352 × 190
3.0T Philips (14 cases)	T2WI-FS	1250	70	380 × 400	320 × 224
	T1WI-DCE	3	1.4	380 × 400	320 × 224

https://doi.org/10.2147/CMAR.S486561

delayed phase (DP). Enhanced scanning involved injecting Gd-diethylenetriamine pentametric acid (Gd-DTPA) at 0.2 mmol/kg with a flow rate of 2.0 mL/s into the anterior elbow vein. Imaging collected during the arterial phase (15–20 s), portal vein phase (50–60 s), and delayed phase (150–180 s).

Image Acquisition and Segmentation

Abdominal-enhanced MRI images of enrolled patients were exported in DICOM format and processed according to IBSI standards.[9] Two interventional physicians with over 8 years of experience in liver cancer diagnosis and treatment used ITK-SNAP software (Version 4.0.2) to manually delineate the region of interest (ROI) (Figure 2). The segmented ROIs were then integrated into a three-dimensional volume of interest (VOI) using software processing. The accuracy of the segmentation results was verified by an associate chief physician specializing in abdominal imaging diagnosis. Intraclass correlation coefficients (ICC) were calculated based on measurements from 30 randomly selected patients to ensure the repeatability and reproducibility of the ICC > 0.8, indicating high consistency.

Feature Extraction and Selection

Before feature extraction, all image sequences were first resampled to a uniform physical spacing of 1 mm × 1 mm × 1 mm. Subsequently, the images were normalized by subtracting the mean intensity value and dividing by the standard deviation. Pyradiomics software (https://pyradiomics.eadthedocs.io/en/latest/features) was used to outline the ROI of the MRI image sequence for feature extraction. Overall, 1688 image features were extracted from each ROI, categorized into (1) intensity statistical features (a universal measure to quantitatively describe voxel intensity distribution in MRI images), (2) shape and size characteristics (reflecting the shape and size of the ROI), (3) texture features (quantifying heterogeneity difference using Gray Level Run-Length Matrix and Gray Level Co-occurrence Matrix within the ROI), and (4) high-order statistical features (obtained by recalculating the intensity and texture after applying various filters such as exponent, logarithm, square, square root, and wavelet transformations).

The patients were randomly assigned in an 8:2 ratio to the training and validation sets. Three methods were employed to reduce the dimensionality of the radiomics features to prevent issues such as model overfitting and multicollinearity. First, the variance threshold method was used to eliminate features with thresholds < 0.8. Second, nonsignificant features ($p > 0.05$) were removed using univariate selection. Last, the least absolute shrinkage and selection operator (LASSO) was used to select the resistance to the most relevant conventional indicators and determine their index weights. Following these dimensionality reduction methods, the radiomics score for each patient (T2WI-FS_RadScore, AP_RadScore, VP_RadScore, and DP_RadScore) was computed using the radiomics scoring formula and integrated into the subsequent model construction.

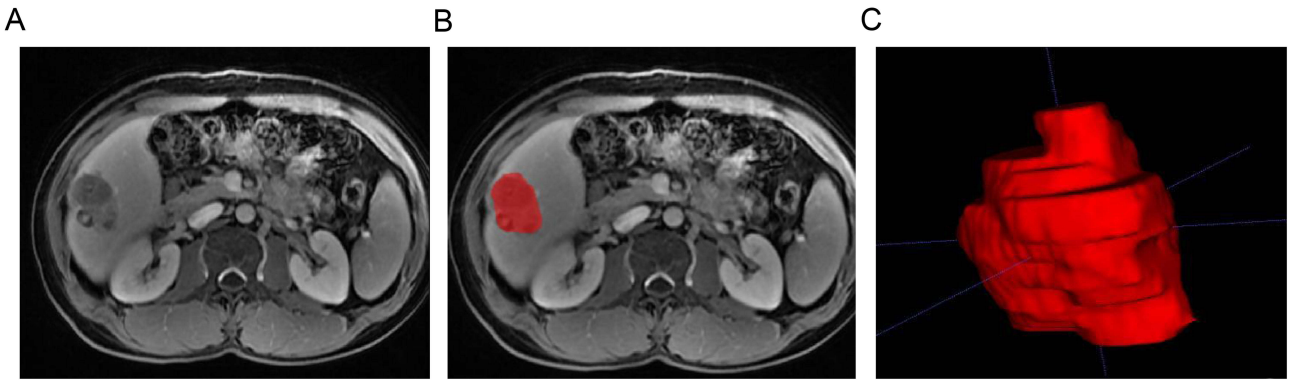

Figure 2 (**A**–**C**) Manual segmentation was conducted to obtain the target tumor ROI: (**A**) delayed phase; (**B**) ROI delineation sample; (**C**) sample of a three-dimensional VOI through software processing. The red-shaded areas in the figures represent regions demarcated via manual segmentation on MRI scans.

Model Construction and Evaluation

Radiomics models were constructed using combinations of multiple sequences and single sequences. This included four models of single sequence models (T2WI-FS, AP, VP, and DP) and three combined sequence models (AP + VP, AP + VP + DP, and T2WI-FS + AP + VP + DP). The clinical features of the patients were collected, and significant features were selected through univariate and multifactorial analyses. Then based on these features, a clinical model (CLnc) and a clinical-radiomics combined model were constructed. Machine learning (ML) methods were used to distinguish HCC TACE refractoriness in model construction. Four ML algorithms, namely support vector machine (SVM), random forest (RF), logistic regression (LR), and adaptive boosting (AdaBoost), were used to construct the model in the training set. Receiver operating characteristic (ROC) curves of area under curve (AUC), accuracy, sensitivity, specificity, and were used to evaluate the classification result.

The nomogram intuitively and concisely reflects the influence of factors predicting TACE refractoriness in patients with HCC, confirming the pivotal role of radiomics characteristics. Calibration curves were used to evaluate the consistency between the model prediction of TACE refractoriness in patients with HCC and the actual TACE refractoriness to HCC.

Statistical Analysis

Statistical analysis was conducted using R software Version 4.3.2 to process clinical and imaging data. For categorical variables, Chi-square tests with continuous corrections were applied. For normally distributed continuous variables, univariate analysis of variance was used. Non-normally distributed continuous variables were analyzed using Kruskal–Wallis rank sum tests. Python software (Version 3.7.0) was used for radiomics feature extraction (Pyradiomics 3.0.1) and feature selection, while the open-source sklearn 1.0.2 library was used for model training and evaluation. ROC curves were generated to calculate the AUC of all models and the DeLong method was used for comparison. Model prediction efficiency was assessed based on accuracy, sensitivity, specificity and F1-score. A significance level of $p < 0.05$ was considered statistically significant.

Results

Patients' Characteristics

Between January 1, 2017, and December 31, 2022, a total of 551 hepatocellular carcinoma (HCC) patients receiving transarterial chemoembolization (TACE) as initial therapy were screened. After applying inclusion and exclusion criteria (Figure 1), 131 eligible patients were enrolled, including 83 TACE-responsive patients and 48 TACE-refractoriness patients. These patients were randomly stratified into a training cohort (n=104) and a validation cohort (n=27) at an 8:2 ratio to ensure balanced group allocation. Baseline characteristics of both cohorts are summarized in Table 2. Comparative analysis revealed no statistically significant differences in clinical-imaging parameters between the training and validation sets (P>0.05), confirming the homogeneity of the datasets.

Clinical Imaging Features and Construction of the CLnc Model

Univariate and multivariate analyses showed that tumor location (odds ratio [OR] = 2.76, $p = 0.04$) and initial TACE efficacy (OR = 6.73, $p < 0.001$) were independent risk factors for TACE refractoriness. Four ML algorithms (SVM, RF, LR, and AdaBoost) were used to construct and evaluate the CLnc model. The results demonstrated strong predictive performance for TACE refractoriness (training set AUC values = 0.876–0.888). The Adaboost algorithm also demonstrated comparable performance, achieving an AUC of 0.888 (95% confidence interval [CI]: 0.842–0.940) in the training set and 0.868 (95% CI: 0.786–0.971) in the validation set. (Tables 3 and 4).

Construction of Radiomics Model

The radiomics model was constructed using four-phase MRI images, combining various sequences: four single-sequence models (T2WI-FS, AP, VP, and DP); three combined models of two sequences (AP + VP); three sequences (AP + VP + DP); and four sequences (T2WI-FS + AP + VP + DP). Dimensionality reduction methods identified 9, 7, 26, 9 and 13,

Table 2 Baseline Characteristics of Enrolled Patients

Clinical-Imaging Features	Train (n=104)	Validation (n=27)	P-value
Gender (Male/female)	85 (81.7)/19 (18.3)	21 (77.8)/6 (22.2)	0.849
Age /(y)	56.44±9.12	55.07±7.63	0.475
Background liver disease (Others/Hepatitis B virus)	20 (19.2)/52 (50.0)	4 (14.8)/16 (59.3)	0.687
AFP/ (ng/mL) (<400/≥400)	65 (62.5)/39 (37.5)	15 (55.6)/12 (44.4)	0.661
AST/ (IU/L)	37.95 [27.98, 52.85]	45.00 [30.20, 54.10]	0.381
ALT/ (IU/L)	31.60 [20.95, 44.50]	34.00 [19.10, 42.90]	0.937
GGT/ (IU/L)	88.35 [49.00, 152.75]	89.00 [53.00, 145.50]	0.905
Albumin (g/dL)	37.04±5.02	37.07±6.18	0.977
Total bilirubin/ (umol/L)	15.15 [11.47, 22.22]	18.60 [14.95, 26.55]	0.064
Creatinine/ (μmol/L)	76.55 [65.53, 89.00]	68.10 [57.10, 85.70]	0.108
Prothrombin time/s	14.40 [13.78, 15.50]	14.60 [13.75, 15.15]	0.659
Platelet count/10^9/L	123.00 [74.75, 175.00]	100.00 [55.50, 128.50]	0.096
CNLC (Ia/Ib/IIa/IIb/IIIa)	37 (35.6)/17 (16.3)/10 (9.6)/11 (10.6)/29 (27.9)	9 (33.3)/7 (25.9)/3 (11.1)/1 (3.7)/7 (25.9)	0.683
BCLC (A/B/C)	53 (51.0)/22 (21.2)/29(27.8)	16 (59.3)/4 (14.8)/7 (25.9)	0.745
Child-Pugh Score (5/6/7/8/9)	60 (57.7)/25 (24.0)/10 (9.6)/3 (2.9)/6 (5.8)	15 (55.6)/6(22.2)/0 (0.0)/4 (14.8)/2 (7.4)	0.077
MELD Score	6.00 [4.00, 8.00]	6.00 [4.00, 8.50]	0.954
ALBI Grade (Level 1 / Level 2/Level 3)	36 (34.6)/64 (61.5)/4 (3.8)	8 (29.6)/18 (66.7)/1 (3.7)	0.883
EOCG Score (0/1)	53 (51.0)/51 (49.0)	18 (66.7)/9 (33.3)	0.214
Number (single / 2 ~ 3/≥ 4)	65 (62.5)/19 (18.3)/20 (19.2)	18 (66.7)/6 (22.2)/3 (11.1)	0.595
Size (maximum tumor diameter)	4.70 [2.80, 7.72]	5.20 [2.60, 8.10]	0.936
Location (peripheral/central/both)	64 (61.5)/22 (21.2)/18 (17.3)	22 (81.5)/2 (7.4)/3 (11.1)	0.134
Morphology (quasi-round/irregular/irregular multinodular fusion)	45 (43.3)/33 (31.7)/26 (25.0)	17 (63.0)/6 (22.2)/4 (14.8)	0.185
Vascular invasion[1] (no or undetectable or simple vascular fistula/Cheng'sClassificationTypeI/Cheng'sClassification TypeII/Cheng'sClassification TypeIII/invasion of hepatic veins)	77 (74.0)/3 (2.9)/14 (13.5)/4 (3.8)/6 (5.8)	20 (74.1)/1 (3.7)/4 (14.8)/1 (3.7)/1 (3.7)	0.993
Enhancement patterns[10] (type 1 or 2/type 3/type 4)	20 (19.2)/57 (54.8)/27 (26.0)	4 (14.8)/10 (37.0)/13 (48.1)	0.129
Intratumoral hemorrhage (no / yes)	69 (66.3)/35 (33.7)	17 (63.0)/10 (37.0)	0.918
Intratumoral lipid (no / yes)	76 (73.1)/28 (26.9)	21 (77.8)/6 (22.2)	0.803
Capsule intact (no / yes)	73 (70.2)/31 (29.8)	15 (55.6)/12 (44.4)	0.225
Intratumoral vascular penetration (no / yes)	76 (73.1)/28 (26.9)	20 (74.1)/7 (25.9)	1
Obvious extratumoral blood supply (no/ yes)	56 (53.8)/48 (46.2)	17 (63.0)/10 (37.0)	0.527
Peritumoral enhancement (no / yes)	72 (69.2)/32 (30.8)	22 (81.5)/5 (18.5)	0.308
Number of intrahepatic metastases (no / yes)	82(78.8)/22(21.2)	22(81.5)/5(18.5)	0.504
Six-and-twelve (<6/6-12/≥12)	47 (45.2)/32 (30.8)/25(22.8)	13 (48.1)/8 (29.6)/6(22.3)	0.504
First TACE effect (CR/PR/SD/PD)	22 (21.2)/54 (51.9)/12 (11.5)/16 (15.4)	6 (22.2)/16 (59.3)/1 (3.7)/4 (14.8)	0.669
Two TACE methods (all c-TACE or CR at the first time/all DEB-TACE or CR at the first time/c-TACE and DEB-TACE respectively)	44 (42.3)/42 (40.4)/18 (17.3)	12 (44.4)/10 (37.0)/5 (18.5)	0.951

Table 3 Univariate and Multivariate Analysis of TACE Refractoriness Clinical-Imaging

Clinical-Imaging Features	Univariate Analysis			Multivariate Analysis		
	OR	95% CI	P-value	OR	95% CI	P-value
Gender (Male/female)	0.97	0.93–1.01	0.12			
Age /(y)	0.37	0.12–0.99	0.06			
Background liver disease (Others/Hepatitis B virus	1.38	0.82–2.36	0.23			
AFP/ (ng/mL) (<400/≥400)	2.74	1.32–5.79	0.01	1.79	0.56–5.72	0.33
AST/ (IU/L)	1.01	1.00–1.02	0.08			
ALT/ (IU/L)	1.01	1.00–1.02	0.11			
GGT/ (IU/L)	1.00	1.00–1.01	0.12			
Albumin (g/dL)	1.02	0.95–1.09	0.66			
Total bilirubin/ (umol/L)	0.99	0.96–1.02	0.59			
Creatinine/ (μmol/L)	1.01	0.99–1.03	0.37			
Prothrombin time/s	0.85	0.68–1.04	0.14			
Platelet count/10^9/L	1.01	1.00–1.02	0.01	1.00	0.99–1.01	0.96
CNLC (Ia/Ib/IIa/IIb/IIIa)	1.61	1.28–2.05	<0.001	0.88	0.30–2.59	0.82
BCLC (A/B/C)	2.06	1.38–3.15	<0.001	1.01	0.22–4.58	0.98
Child-Pugh Score (5/6/7/8/9)	0.70	0.47–0.98	0.04	1.08	0.30–2.59	0.82
MELD Score	0.99	0.91–1.09	0.86			
ALBI Grade (Level 1 / Level 2/Level 3)	0.92	0.47–1.80	0.81			
EOCG Score (0/1)	1.14	0.56–2.34	0.71			
Number (single / 2 ~ 3/≥ 4)	2.27	1.42–3.70	0.01	3.84	0.67–21.88	0.13
Size (maximum tumor diameter)	1.20	1.08–1.34	0.01	1.03	0.72–1.47	0.88
Location (peripheral/central/both)	2.86	1.48–5.90	0.01	2.76	1.02–7.46	0.04
Morphology(quasi-round/irregular/irregular multinodular fusion)	2.72	1.70–4.49	<0.001	0.94	0.37–2.37	0.90
Vascular invasion[1] (no or undetectable or simple vascular	1.63	1.20–2.28	0.01	1.31	0.58–2.98	0.52
Fistula/Cheng'sClassificationTypeI/Cheng'sClassification TypeII/Cheng'sClassification TypeIII/ invasion of hepatic veins)						
Enhancement patterns[10] (type 1or 2/type 3/type 4)	1.58	0.95–2.71	0.08			
Intratumoral hemorrhage (no / yes)	1.24	0.59–2.61	0.56			
Intratumoral lipid(no / yes)	1.81	0.81–4.02	0.15			
Capsule intact(no / yes)	0.07	0.02–0.22	<0.001	0.36	0.06–2.12	0.26
Intratumoral vascular penetration(no / yes)	2.33	1.06–5.18	0.04	1.84	0.43–7.85	0.41
Obvious extratumoral blood supply(no/ yes)	3.78	1.81–8.14	<0.001	2.46	0.56–10.76	0.23
Peritumoral enhancement(no / yes)	4.53	2.05–10.38	<0.001	2.87	0.76–10.76	0.12
Number of intrahepatic metastases(no / yes)	2.56	1.52–4.60	0.01	0.57	0.11–2.91	0.50
Six-and-twelve (<6/6-12/≥12)	2.70	1.69–4.45	<0.001	0.49	0.10–2.35	0.37
First TACE effect (CR/PR/SD/PD)	6.35	3.45–13.82	<0.001	6.73	2.72–16.65	<0.001
Two TACE methods (all c-TACE or CR at the first time/all DEB-TACE or CR at the first time/c-TACE and DEB-TACE respectively)	1.54	0.95–2.53	0.08			

Table 4 Prediction Performance of Each Model in Training Set and Validation Set

Model Type	Train					Validation				
	Accuracy	Sensitivity	Specificity	AUC(95% CI)	*F1-score*	Accuracy	Sensitivity	Specificity	AUC(95% CI)	*F1-score*
Adaboost T2WI-FS	0.731	0.789	0.697	0.807(0.738–0.864)	0.682	0.704	0.700	0.706	0.738(0.602–0.861)	0.636
AP	0.731	0.684	0.758	0.772(0.699–0.835)	0.650	0.741	0.600	0.824	0.715(0.693–0.827)	0.632
VP	0.788	0.658	0.864	0.861(0.804–0.914)	0.694	0.815	0.800	0.824	0.797(0.664–0.929)	0.762
DP	0.702	0.789	0.652	0.750(0.682–0.819)	0.659	0.593	0.600	0.588	0.603(0.489–0.720)	0.522
AP+VP	0.760	0.579	0.864	0.837(0.769–0.895)	0.638	0.741	0.800	0.706	0.809(0.671–0.938)	0.696
AP+VP+DP	0.788	0.763	0.803	0.856(0.791–0.914)	0.725	0.778	0.600	0.882	0.803(0.702–0.908)	0.667
AP+VP+DP+T2WI-FS	0.808	0.895	0.758	0.890(0.843–0.936)	0.773	0.778	0.900	0.706	0.835(0.733–0.934)	0.750
CLnc model	0.837	0.789	0.864	0.888(0.842–0.940)	0.779	0.815	0.600	0.941	0.868(0.786–0.971)	0.706
Combined model	0.875	0.763	0.939	0.939(0.908–0.974)	0.817	0.815	0.800	0.824	0.891(0.821–0.952)	0.762

(*Continued*)

Table 4 (Continued).

Model Type	Train					Validation				
	Accuracy	Sensitivity	Specificity	AUC(95% CI)	*F1-score*	Accuracy	Sensitivity	Specificity	AUC(95% CI)	*F1-score*
RF T2WI-FS	0.779	0.684	0.833	0.838(0.771–0.893)	0.693	0.778	0.600	0.882	0.744(0.611–0.871)	0.667
AP	0.712	0.553	0.803	0.785(0.703–0.851)	0.583	0.667	0.600	0.706	0.715(0.696–0.821)	0.571
VP	0.779	0.500	0.939	0.855(0.782–0.914)	0.623	0.778	0.500	0.941	0.812(0.679–0.949)	0.625
DP	0.750	0.632	0.818	0.801(0.727–0.870)	0.649	0.741	0.400	0.941	0.712(0.581–0.839)	0.533
AP+VP	0.817	0.684	0.894	0.863(0.797–0.920)	0.732	0.667	0.600	0.706	0.829(0.721–0.929)	0.571
AP+VP+DP	0.740	0.553	0.848	0.825(0.752–0.882)	0.609	0.667	0.600	0.706	0.788(0.684–0.881)	0.571
AP+VP+DP+T2WI-FS	0.817	0.895	0.773	0.889(0.842–0.932)	0.782	0.741	0.700	0.765	0.835(0.727–0.938)	0.667
CLnc model	0.808	0.605	0.924	0.876(0.828–0.931)	0.697	0.815	0.500	1.000	0.856(0.774–0.966)	0.667
Combined model	0.865	0.684	0.970	0.951(0.915–0.977)	0.788	0.778	0.400	1.000	0.871(0.810–0.933)	0.667
LR T2WI-FS	0.702	0.763	0.667	0.808(0.736–0.873)	0.652	0.778	0.700	0.824	0.794(0.662–0.929)	0.700
AP	0.644	0.711	0.606	0.761(0.687–0.838)	0.593	0.630	0.800	0.529	0.724(0.705–0.829)	0.615
VP	0.779	0.921	0.697	0.896(0.843–0.941)	0.753	0.741	0.800	0.706	0.853(0.727–0.965)	0.696
DP	0.692	0.737	0.667	0.765(0.689–0.845)	0.636	0.778	0.800	0.765	0.735(0.617–0.850)	0.727
AP+VP	0.750	0.842	0.697	0.823(0.764–0.881)	0.711	0.741	0.900	0.647	0.847(0.737–0.953)	0.720
AP+VP+DP	0.760	0.763	0.758	0.850(0.791–0.905)	0.699	0.704	0.700	0.706	0.847(0.737–0.954)	0.636
AP+VP+DP+T2WI-FS	0.817	0.895	0.773	0.905(0.853–0.949)	0.782	0.778	0.700	0.824	0.876(0.773–0.976)	0.700
CLnc model	0.837	0.789	0.864	0.885(0.835–0.940)	0.779	0.815	0.600	0.941	0.868(0.786–0.971)	0.706
Combined model	0.885	0.921	0.864	0.955(0.918–0.984)	0.854	0.852	0.900	0.824	0.941(0.880–0.991)	0.818
SVM T2WI-FS	0.788	0.526	0.939	0.871(0.806–0.921)	0.645	0.704	0.500	0.824	0.812(0.691–0.938)	0.556
AP	0.788	0.632	0.879	0.858(0.792–0.918)	0.686	0.630	0.900	0.471	0.735(0.623–0.846)	0.643
VP	0.740	0.421	0.924	0.863(0.802–0.919)	0.542	0.852	0.800	0.882	0.859(0.734–0.979)	0.800
DP	0.721	0.500	0.848	0.820(0.758–0.884)	0.567	0.593	0.500	0.647	0.759(0.625–0.889)	0.476
AP+VP	0.788	0.658	0.864	0.894(0.839–0.942)	0.694	0.704	0.900	0.588	0.859(0.743–0.968)	0.692
AP+VP+DP	0.779	0.500	0.939	0.853(0.798–0.914)	0.623	0.667	0.700	0.647	0.841(0.733–0.955)	0.609
AP+VP+DP+T2WI-FS	0.769	0.526	0.909	0.892(0.837–0.938)	0.625	0.741	0.700	0.765	0.865(0.762–0.960)	0.667
CLnc model	0.837	0.789	0.864	0.877(0.826–0.932)	0.779	0.815	0.600	0.941	0.868(0.786–0.971)	0.706
Combined model	0.856	0.816	0.879	0.939(0.901–0.973)	0.805	0.815	0.800	0.824	0.891(0.879–0.917)	0.778

17, and 20 characteristics associated with TACE refractoriness, respectively. Four ML algorithms were used to construct four prediction models, resulting in a total of 28 radiomics models. The Logistic Regression (LR) algorithm demonstrated the best performance in constructing the T2WI-FS + AP + VP + DP combined model, achieving AUC values of 0.905 (95% confidence interval [CI]: 0.853–0.949) in the training set and 0.876 (95% CI: 0.773–0.976) in the validation set. It also showed optimal performance in the single-sequence VP model, with AUC values reaching 0.896 (95% CI: 0.843–0.941) in the training set and 0.853 (95% CI: 0.727–0.965) in the validation set (Table 4 and Figure 3).

Construction of the Combined Model

The combined model was constructed by integrating four algorithms using the optimal radiomics label and clinical image features. The results demonstrated superior prediction performance compared to other models (training set AUC range = 0.939–0.955). The LR algorithm demonstrated superior performance, achieving AUC values of 0.955 (95% CI: 0.918–0.984) in the training set and 0.941 (95% CI: 0.880–0.991) in the validation set, both fully meeting the criteria for robust predictive capability (Table 4 and Figure 4). Comparative analysis of classifier algorithms based on the combined model revealed no statistically significant differences between classifiers ($P>0.05$). Furthermore, longitudinal comparison between the LR combined model (demonstrating superior validation set performance) and other LR models showed statistically significant differences in outcomes ($P<0.05$)(Table 5).

Establishment and Verification of the Nomogram Model

The nomogram model was established by integrating the above-determined radiomics labels and clinical image features (Figure 5). The results indicated strong associations between radscores, initial TACE efficacy, and tumor location with TACE refractoriness in patients with HCC. Calibration curves demonstrated high consistency between model prediction

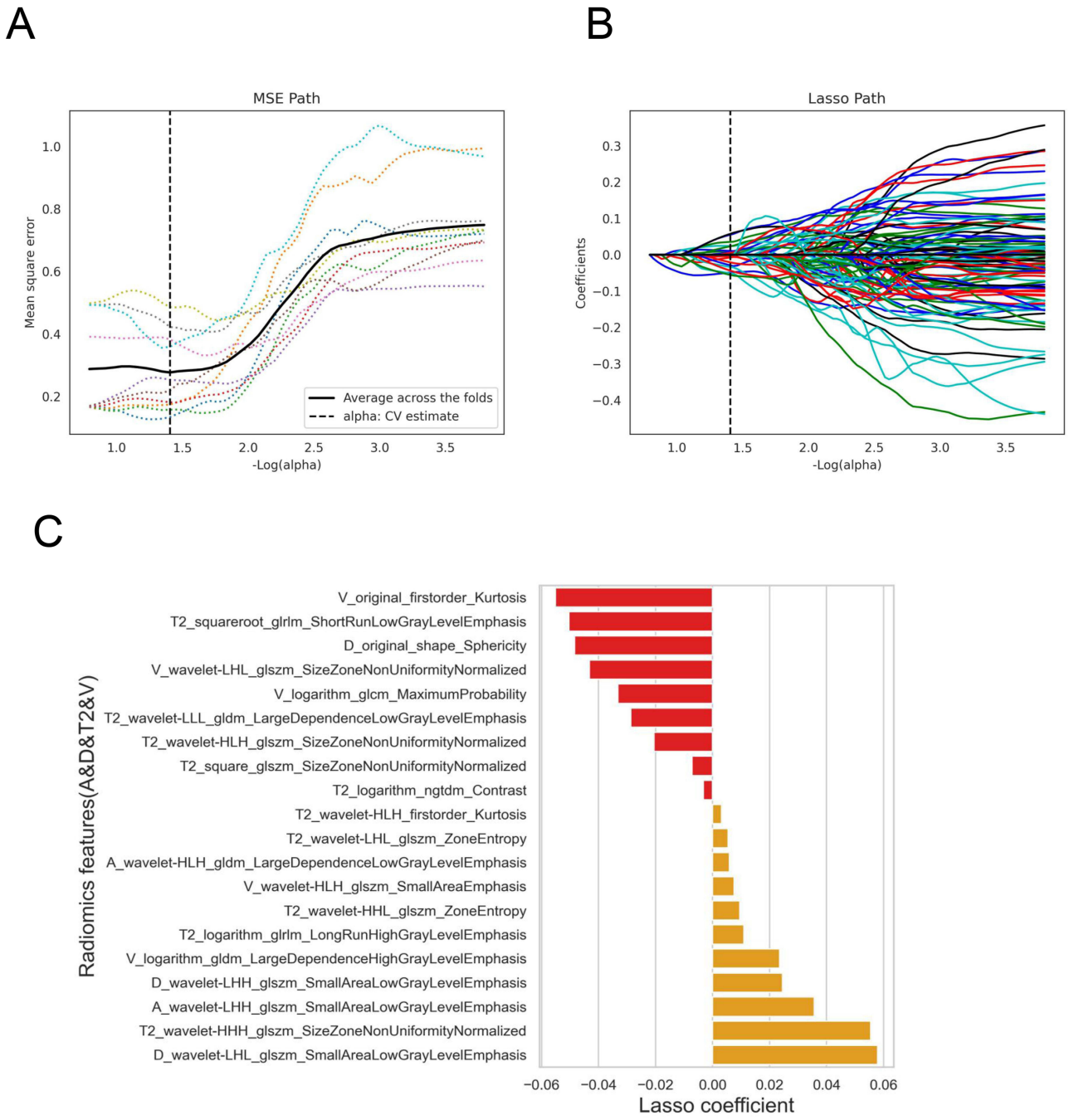

Figure 3 (**A**–**C**) The LASSO algorithm was used to select characteristic process maps from the MRI-AP + VP + DP + T2WI-FS four-sequence images. (**A**) In the LASSO regression model, 10-fold cross-validation was used to choose the best tuning parameter, −log(α) = 1.45; (**B**) λ yielded 20 non-zero coefficient radiomics features; (**C**) The characteristic coefficient diagram shows 20 radiologic features and their corresponding LASSO coefficients.

and actual outcomes in both the training and validation sets, indicating their clinical reliability (Figure 6). Decision curves showed that the integrated model was superior to the radiomics and CLnc models (Figure 7).

Comparative Performance of Machine Learning Models for Treatment Response Prediction

Table 4 presents the results from the four algorithms. Among which the AUC is better: the SVM algorithm constructed four models (T2WI-FS, AP, DP, and AP + VP) with AUC ranges of 0.820–0.939 for the training set and 0.759–0.891 for

https://doi.org/10.2147/CMAR.S486561

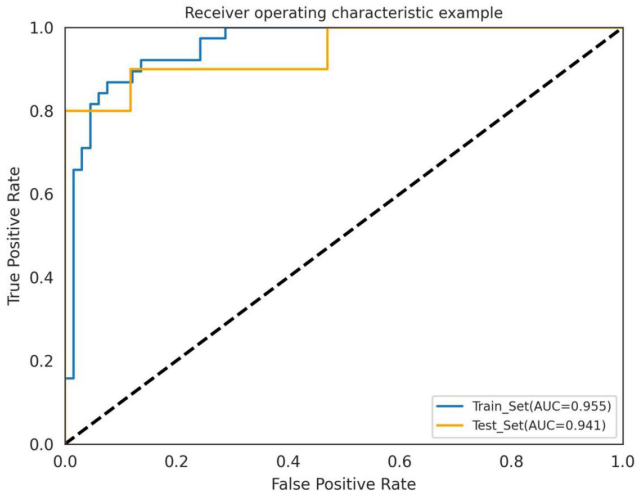

Figure 4 Construction of the ROC curve of the combined model using the LR algorithm.

the validation set, Two models (CLnc and AP + VP + DP) were constructed using the AdaBoost algorithm, with AUC ranges of 0.750–0.939 for the training set and 0.603–0.891 for the validation set, The LR algorithm produced three models (VP, AP + VP + DP + T2WI-FS, combined) with AUC ranges of 0.761–0.955 for the training set and 0.724–0.941 for the validation set. The combined sequence outperformed the CLnc model in predictive performance. The AP + VP + DP + T2WI-FS model had the best performance in the radiomics model, with the radscore violin plot depicted in Figure 8. The combined model had the highest diagnostic efficiency, with the LR algorithm achieving the best performance, boasting AUC values of 0.955 for the training set and 0.941 for the validation set.

Discussion

The definition of TACE refractoriness varies across countries. The latest expert consensus in China suggests focusing only on the TACE target lesion rather than considering the entire disease comprehensively. This approach aims to enhance the understanding of the efficacy of local TACE target lesions and mitigate subjective factors that could diminish the therapeutic effects. However, HCC is increasingly recognized as a systemic disease, underscoring the importance of a comprehensive evaluation for prognosis. Therefore, despite these considerations, the traditional concept of TACE refractoriness[3] remains the prevailing research standard in this field.

In this study, we collected and extracted radiomics and clinical imaging features from four MRI scan sequences. Nine sets of radiomics features were formed separately and combined. After dimensionality reduction, we constructed 36 radiomics models by integrating four ML algorithms and compared their predictive efficacy for TACE refractoriness by calculating the AUC from ROC curves. The best-performing model selected for the final screening combined clinical

Table 5 Contrasted Results of Combined Models

Model Comparison	P-value	
	Train	Validation
Combined_LR model vs Combined_RF model	0.928	0.843
Combined_LR model vs Combined_SVM model	0.273	0.623
Combined_LR model vs Combined _ADA model	0.520	0.363
Combined _LR model vs AP+VP+DP+T2WI-FS_LR model	0.013	0.043
Combined_LR model vs AP+VP+DP_LR model	0.001	0.027
Combined_LR model vs AP+VP_LR model	<0.001	0.048
Combined_LR model vs VP_LR model	0.021	0.041
Combined_LR model vs Clnc_LR model	0.005	0.047

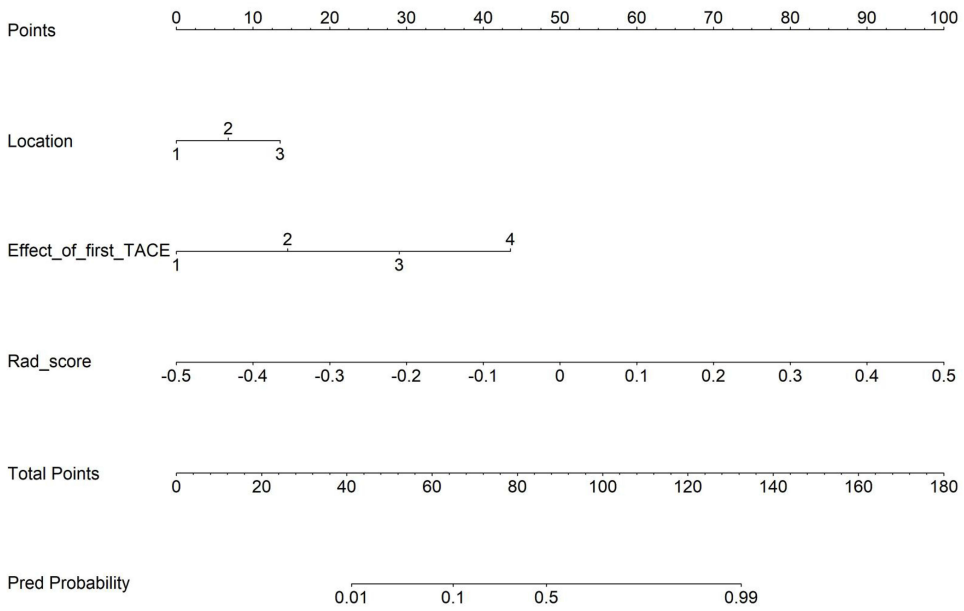

Figure 5 Nomogram model for predicting HCC TACE refractoriness.

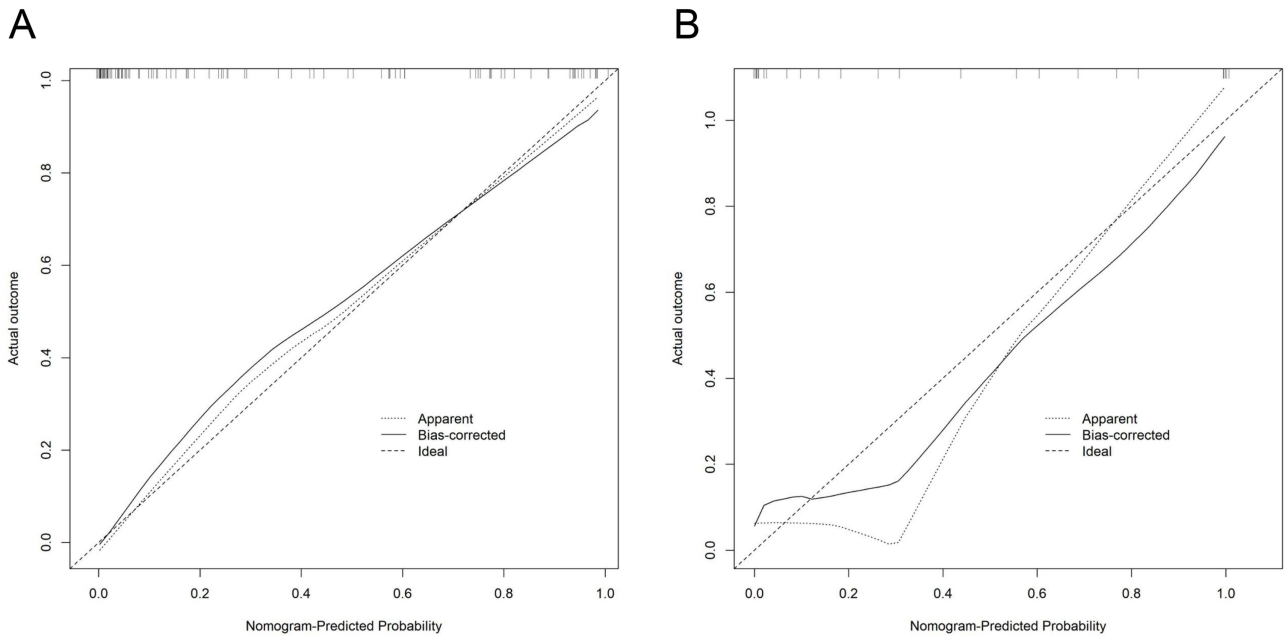

Figure 6 (**A** and **B**) Calibration curve of the prediction model. (**A**) Training; (**B**) Validation.

imaging and radiomics features. The AUC values of the training and validation sets were 0.955 and 0.941, respectively, indicating strong predictive efficiency. This model demonstrates superior efficacy compared to previous studies on TACE refractoriness prediction models.[11–13] It provides crucial support for precision medicine in the early identification of TACE refractoriness, suggesting timely treatment optimization to prevent poor prognosis and liver function damage due to repeated TACE treatment. The calibration curve was used to verify the prediction consistency of the model prediction results with the actual outcomes, indicating that the prediction performance of the combined model was reliable. Conversely, the decision curves demonstrated superiority over the radiomics and CLnc models.

https://doi.org/10.2147/CMAR.S486561

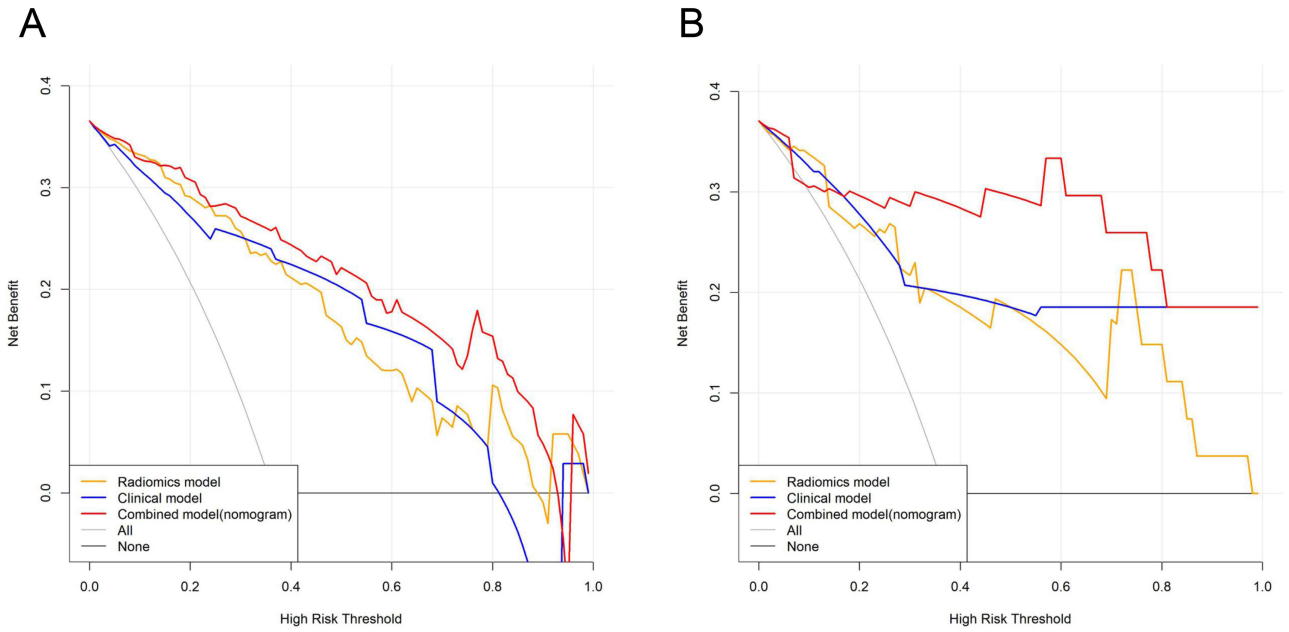

Figure 7 (**A** and **B**) Decision curves of each model for the training and validation sets. (**A**) Training; (**B**) Validation.

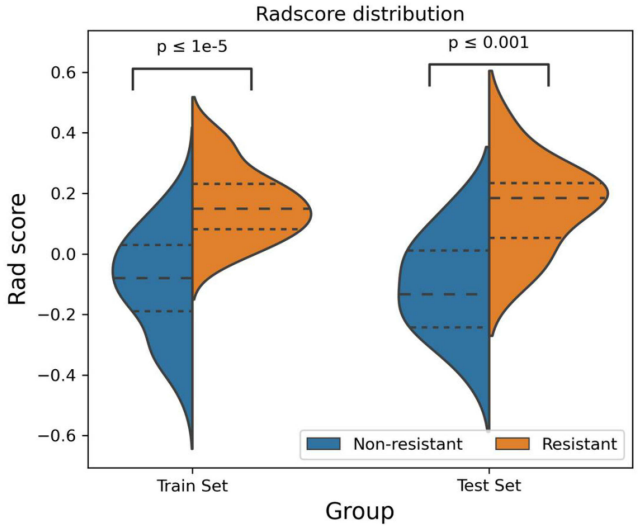

Figure 8 Radscore distribution.

TACE treatment is widely used in patients with HCC across different stages, but tumor heterogeneity results in significant variations in prognosis after TACE treatment. Radiomics extracts texture parameters from the entire target tumor image, providing a quantitative evaluation of tumor growth, metastasis, efficacy, and potential heterogeneity. This method is superior to traditional invasive and limited biopsy techniques.[14] The VP model developed using LR demonstrated robust predictive performance for HCC TACE refractoriness, with AUCs of 0.896 (training cohort) and 0.853 (validation cohort). This may be attributed to the clearer internal structure caused by contrast agent clearance in portal vein-stage tumors. Relevant studies have confirmed that an earlier clearance time yields a worse degree of tumor differentiation and that TACE often yields suboptimal results for poorly differentiated liver cancer.[15] Currently, there is no correlation between TACE refractoriness and portal vein clearance. Several studies have shown that the portal vein-

stage prediction model is highly effective in predicting outcomes in patients with HCC following ablation, surgery, and TACE.[7,16,17] However, the LR algorithm or Cox proportional hazards were used only in all cases, and the study results may be biased. Furthermore, a combined analysis of single sequences indicated that the T2WI-FS + AP + VP + DP four-sequence model provided the most accurate prediction performance. Constructing multisequence combinatorial radiomics models is commonly used to enhance the efficiency of current radiomics research. Recent studies have proven that the construction of the CT + MRI + CLnc model outperforms the single clinical model, the single CT model, the single MRI model, or the combined CT + MRI model and can effectively predict PFS (progression-free survival) and OS (overall survival) after HCC surgery.[18] This suggests that combining multiple sequences can offer more abundant tumor information for predicting treatment outcomes.

In this study, clinical imaging features, including the efficacy of the initial TACE and tumor location, were integrated into the CLnc prediction model. The performance of the TACE refractoriness prediction model was not inferior to that of the existing domestic TACE refractoriness prediction model. Based on the training set of the four ML algorithms, the AUC exceeded 0.8. Considering the clinical imaging features, more emphasis was placed on the imaging features rich in tumor information than on previous prediction models. Precision TACE[19] has been widely adopted in clinical practice, effectively reducing false TACE refractoriness caused by technical issues. Therefore, TACE remains the primary treatment choice for unresectable HCC. mRECIST is a standard method for postoperative imaging evaluation of TACE efficacy.[20] Additionally, it was found that tumors located in the central location were more resistant to TACE than peripheral locations. Previous studies have shown that lesion location impacts TACE efficacy, with liver segments I and IV (central locations) demonstrating poorer outcomes, likely due to the difficulty of TACE superselection resulting from the abundant and slender anastomosis branches and vascular variation between the left and right lobes of the liver.[21,22] Other studies have suggested that the distance between the tumor and portal vein bifurcation partially affects TACE efficacy.[23]

This study also found that single-sequence and multisequence optimal models were constructed using the LR algorithm. Previous studies have established LR as the most widely used ML algorithm in HCC radiomics, capable of predicting postoperative efficacy and survival[7] and HCC TACE refractoriness. In conclusion, LR was used to construct a combined radiomics prediction model of tumor location combined with initial treatment and the therapeutic effect of the first TACE treatment, which can effectively identify patients with HCC TACE refractoriness early and noninvasively.

Four different MRI scanners were used in this study, and the MRI radiomics model studied will have extensive applicability and more accurately reflect the real clinical world. Images were standardized before feature extraction to reduce bias in the experimental results. This study not only increased the proportion of image features that better reflect tumor information in preoperative observation indicators but also expanded upon previous studies by comparing multiple ML algorithms and sequence models. In other words, multiple ML algorithms across MRI multisequences were used to construct radiomics models of multiple single sequences and multiple combinations of multiple sequences. This study achieved the best results in predicting HCC TACE refractoriness, with the combined model demonstrating broader applicability (AUC > 0.9). Calibration and decision curve analyses showed that the model predicted TACE refractoriness with high relevance to the actual outcomes. The combined radiomics model had the best predictive efficiency, which was significant for the radiomics biological phenotype. This finding has practical clinical implications for the early identification of TACE refractoriness in patients with HCC, facilitating the optimization of treatment plans in advance and the prevention of disease progression and liver function damage due to ineffective therapy. Identifying patients with a good therapeutic response to TACE can enhance its therapeutic effects and benefits.

Several limitations were observed in our study. First, this single-center retrospective study lacked external validation and prospective studies. We plan to address these limitations in future studies by conducting multicenter external validation experiments to further evaluate the generalibility and robustness of our radiomics model. Second, the standardization of the radiomics features could not mitigate bias from various scanning devices and manual segmentation of the target tumor regions. Finally, interpreting the complex relationship between imaging features and tumor heterogeneity based on big data extraction presents a significant challenge. Further research addressing HCC TACE refractoriness should focus on exploring the biological mechanisms of target tumors using radiomics features.

Conclusion

In this study, the prediction performance of multiple radiomics models for HCC TACE refractoriness was as follows: the VP of single sequence model was better than that of single sequence model, and the combination of T2WI-FS + AP + VP + DP was the best. The joint radiomics model constructed based on the best multisequence combination of radiomics features and clinical imaging features achieved optimal performance among the four algorithms, among which the LR algorithm performed best and is expected to be an effective tool for predicting HCC TACE refractoriness.

Data Sharing Statement

All the data generated and analyzed during this study are included in our manuscript. The data supporting the findings of this study are available from the corresponding author upon reasonable request.

Ethics Approval and Informed Consent

The study was conducted according to the guidelines of the Declaration of Helsinki and approved by the Ethics Committee of the First Affiliated Hospital of Kunming University.

Acknowledgments

The author thank Yaying Yang (Medical Imaging Department, The First Affiliated Hospital of Kunming Medical University) in the study for her support and assistance.

Author Contributions

All authors made a significant contribution to the work reported, whether that is in the conception, study design, execution, acquisition of data, analysis and interpretation, or in all these areas; took part in drafting, revising or critically reviewing the article; gave final approval of the version to be published; have agreed on the journal to which the article has been submitted; and agree to be accountable for all aspects of the work.

Funding

This article is supported by the Clinical Medical Research Center of Radiology and Therapy of Yunnan Province (No. Z-202102AA100067).

Disclosure

The authors report no conflicts of interest in this work.

References

1. Zhou J, Sun H, Wang Z, et al. Guidelines for the diagnosis and treatment of primary liver cancer; 2022 edition. *Liver Cancer*. 2023;12(5):405–444. doi:10.1159/000530495
2. Kim J, Sinn DH, Choi MS, et al. Hepatocellular carcinoma with extrahepatic metastasis: are there still candidates for transarterial chemoembolization as an initial treatment? *PLoS One*. 2019;14(3):e0213547. doi:10.1371/journal.pone.0213547
3. Kudo M, Matsui O, Izumi N, et al. Transarterial chemoembolization failure/refractoriness: JSH-LCSGJ criteria 2014 update. *Oncology*. 2014;87 (suppl 1):22–31. doi:10.1159/000368142
4. Cheng AL, Amarapurkar D, Chao Y, et al. Re-evaluating transarterial chemoembolization for the treatment of hepatocellular carcinoma: consensus recommendations and review by an International Expert Panel. *Liver Int*. 2014;34(2):174–183. doi:10.1111/liv.12314
5. Raoul JL, Gilabert M, Piana G. How to define transarterial chemoembolization failure or refractoriness: a European perspective. *Liver Cancer*. 2014;3(2):119–124. doi:10.1159/000343867
6. Clinical Guidelines Committee of Chinese College of Interventionalists. Expert consensus on the TACE failure/refractoriness and its subsequent therapies in treating patients with hepatocellular carcinoma. *J Interv Radiol*. 2022;31(11):1039–1044.
7. Zhao Y, Wang N, Wu J, et al. Radiomics analysis based on contrast-enhanced MRI for prediction of therapeutic response to transarterial chemoembolization in hepatocellular carcinoma. *Front Oncol*. 2021;11:582788. doi:10.3389/fonc.2021.582788
8. Yi Z, Zhi XZ. Chinese clinical practice guidelines for transarterial chemoembolization of hepatocellular carcinoma; 2023 edition. *Natl Med J China*. 2023;103(34):2674–2694.
9. Bettinelli A, Branchini M, De Monte F, Scaggion A, Paiusco M. Technical Note: an IBEX adaption toward image biomarker standardization. *Med Phys*. 2020;47(3):1167–1173. doi:10.1002/mp.13956

10. Kawamura Y, Ikeda K, Seko Y, et al. Heterogeneous type 4 enhancement of hepatocellular carcinoma on dynamic CT is associated with tumor recurrence after radiofrequency ablation. *AJR Am J Roentgenol*. 2011;197(4):W665–W673. doi:10.2214/AJR.11.6843
11. Yang C. *Prognostic Analysis of TACE Resistance in Hepatocellular Carcinoma and the Value of AI-Based with Whole-Liver MRI Radiomics in Predicting the Patients' Prognosis*. 2023. 2023.000107.Chinese. Peking Union Medical College
12. Xu X. *Machine Learning-Based Radiomics Analysis of CT and MRI for Prediction of Hepatocellular Carcinoma Refractory to Conventional Transarterial Chemoembolization*. 2022. 2022.000757.Chinese. Shandong University
13. Na Z, Biao Z, Xiangke N. Establishing combined clinical-imaging nomogram model for early identification of TACE-refractory hepatocellular carcinoma. *Chin J Interv Imaging Ther*. 2022;19(05):263–267.
14. Wang Y, Li M, Zhang Z, Gao M, Zhao L. Application of radiomics in the efficacy evaluation of transarterial chemoembolization for hepatocellular carcinoma: a systematic review and meta-analysis. *Acad Radiol*. 2024;31(1):273–285. doi:10.1016/j.acra.2023.08.001
15. Feng Y, Qin XC, Luo Y, Li YZ, Zhou X. Efficacy of contrast-enhanced ultrasound washout rate in predicting hepatocellular carcinoma differentiation. *Ultrasound Med Biol*. 2015;41(6):1553–1560. doi:10.1016/j.ultrasmedbio.2015.01.026
16. Yuan C, Wang Z, Gu D, et al. Prediction early recurrence of hepatocellular carcinoma eligible for curative ablation using a Radiomics nomogram. *Cancer Imaging*. 2019;19(1):21. doi:10.1186/s40644-019-0207-7
17. Liu Q, Li J, Liu F, et al. A radiomics nomogram for the prediction of overall survival in patients with hepatocellular carcinoma after hepatectomy. *Cancer Imaging*. 2020;20(1):82. doi:10.1186/s40644-020-00360-9
18. He Y, Hu B, Zhu CZ, et al. A novel multimodal radiomics model for predicting prognosis of resected hepatocellular carcinoma. *Front Oncol*. 2022;12(6):745258. doi:10.3389/fonc.2022.745258
19. Jingying M, Agile Y, Zhiping Y. Therapeutic goals and embolic endpoints of fine TACE. *J Surg Concepts Pract*. 2022;27(02):131–133.
20. Llovet JM, Lencioni R. mRECIST for HCC: performance and novel refinements. *J Hepatol*. 2020;72(2):288–306. doi:10.1016/j.jhep.2019.09.026
21. Miki I, Murata S, Uchiyama F, et al. Evaluation of the relationship between hepatocellular carcinoma location and transarterial chemoembolization efficacy. *World J Gastroenterol*. 2017;23(35):6437–6447. doi:10.3748/wjg.v23.i35.6437
22. Weihua Z, Yue H. Research progress of the applied anatomy of the caudate lobe of liver. *Electron J Liver Tumor*. 2023;10(01):45–48.
23. Bryant MK, Dorn DP, Zarzour J, et al. Computed tomography predictors of hepatocellular carcinoma tumour necrosis after chemoembolization. *HPB*. 2014;16(4):327–335. doi:10.1111/hpb.12149